27. Banfi, S. *et al*. Identification and mapping of human cDNAs homologous to Drosophila mutant genes through EST database searches. *Nature Genet.* **13,** 167–174 (1996).
28. Bernal, J., Lee, J.-H., Cribbs, L. L. & Perez-Reyes, E. Full reversal of Pb^{++} block of L-type Ca^{++} channels requires treatment with heavy metal antidotes. *J. Pharmacol. Exp. Ther.* **282,** 172–180 (1997).
29. Lacerda, A. E., Perez-Reyes, E., Wei, X., Castellano, A. & Brown, A. M. T-type and N-type calcium channels of *Xenopus* oocytes: evidence for specific interactions with beta subunits. *Biophys. J.* **66,** 1833–1843 (1994).
30. VanDongen, A. M. J. A new algorithm for idealizing single ion channel data containing multiple unknown conductance levels. *Biophys. J.* **70,** 1303–1315 (1996).

Acknowledgements. We thank J. Yang for expert technical support. We also thank the UK HGMP Resource Centre for the Genbridge 4 radiation hybrid mapping panel and the EUCIB mouse panel. This work was supported by grants from the NIH, Potts Foundation and the Medical Research Council. E.P.-R. is an established investigator of the American Heart Association.

Correspondence and requests for materials should be addressed to E.P.-R. (e-mail: eperez@luc.edu). The α1G sequences have the following Genbank accession numbers: rat, AF027984; human, AF029228 and AF029229. Human gene results are at www.hgmp.mrc.ac.uk/cgi-bin/contig/rhmapper.pl. Mouse gene results are coded as 97/MW/001 at www.hgmp.mrc.ac.uk/Mbx/MbxHomepage.html.

Disruption of IRS-2 causes type 2 diabetes in mice

Dominic J. Withers*†, Julio Sanchez Gutierrez*†, Heather Towery*, Deborah J. Burks*, Jian-Ming Ren‡, Stephen Previs‡, Yitao Zhang*, Dolores Bernal*, Sebastian Pons*, Gerald I. Shulman‡, Susan Bonner-Weir* & Morris F. White*

** Howard Hughes Medical Institute, Joslin Diabetes Center, Department of Medicine, Harvard Medical School, Boston, Massachusetts 02215, USA*
‡ Howard Hughes Medical Institute, Department of Medicine, Yale University School of Medicine, New Haven, Connecticut 06520, USA
† These authors contributed equally to this work.

Human type 2 diabetes is characterized by defects in both insulin action and insulin secretion. It has been difficult to identify a single molecular abnormality underlying these features. Insulin-receptor substrates (IRS proteins) may be involved in type 2 diabetes: they mediate pleiotropic signals initiated by receptors for insulin and other cytokines[1]. Disruption of IRS-1 in mice retards growth, but diabetes does not develop because insulin secretion increases to compensate for the mild resistance to insulin[2,3]. Here we show that disruption of IRS-2 impairs both peripheral insulin signalling and pancreatic β-cell function. IRS-2-deficient mice show progressive deterioration of glucose homeostasis because of insulin resistance in the liver and skeletal muscle and a lack of β-cell compensation for this insulin resistance. Our results indicate that dysfunction of IRS-2 may contribute to the pathophysiology of human type 2 diabetes.

Secretion of insulin from pancreatic β-cells tightly regulates glucose homeostasis by stimulating use of glucose by peripheral tissues and inhibiting hepatic glucose production[4]. Development of type 2 diabetes is characterized by a particular breakdown of this system: hyperinsulinaemia compensates for the resistance to insulin that is found in the early prediabetic state[5]. The subsequent development of hyperglycaemia results from the failure of β-cells to secrete enough insulin for effective compensation[5]. The cellular response to insulin is mediated by tyrosine phosphorylation of several cytosolic docking proteins (IRS proteins), which couple the insulin receptor to various effector molecules, including phosphatidylinositol-3-OH kinase (PI(3)K), Grb2/SOS, SHP2, NCK and CRK[1]. Identification of IRS-2 (ref. 6) as an alternative insulin receptor substrate in IRS-1-deficient mice[7] indicates that this may have an important role in mediating glucose homeostasis. Therefore, to characterize the role of IRS-2 in insulin-mediated regulation of glucose metabolism, we inactivated this gene by homologous recombination (Fig. 1a).

Heterozygous *IRS-2*$^{+/-}$ offspring survived to adulthood and were interbred to homozygosity. Mice lacking IRS-2 were identified by Southern blot analysis, and the absence of IRS-2 was confirmed by western blotting of liver and skeletal muscle tissue extracts (Fig. 1b, c). Analysis of IRS expression in these tissues showed comparable levels of IRS-1 in *IRS-2*$^{-/-}$ and wild-type animals and comparable levels of IRS-2 in *IRS-1*$^{-/-}$ and wild-type mice (Fig. 1d). *IRS-2*$^{-/-}$ neonates were 10% smaller than *IRS-2*$^{+/-}$ or wild-type littermates, and this small difference in weight persisted during weaning and into adult life (Fig. 1e).

Blood sugar levels were analysed at various ages to establish the role of IRS-2 in glucose homeostasis. Three days after birth, levels of randomly fed sugars were elevated in *IRS-2*$^{-/-}$ mice (166 ± 13 mg dl^{-1}) compared with in wild-type mice (116 ± 10 mg dl^{-1}). Monitoring of blood glucose between 3 and 6 weeks of age showed the development of fasting hyperglycaemia in *IRS-2*$^{-/-}$ mice, and at 6–8 weeks of age these mice exhibited marked glucose intolerance during an intraperitoneal glucose-tolerance test (Fig. 2a, b). At 10 weeks, *IRS-2*$^{-/-}$ mice were overtly diabetic with fasting glucose levels of 323 ± 35 mg dl^{-1}, and if left untreated the levels of fasting sugars rose progressively to >400 mg dl^{-1} at 12–16 weeks of age. Male *IRS-2*$^{-/-}$ mice showed polydypsia and polyuria

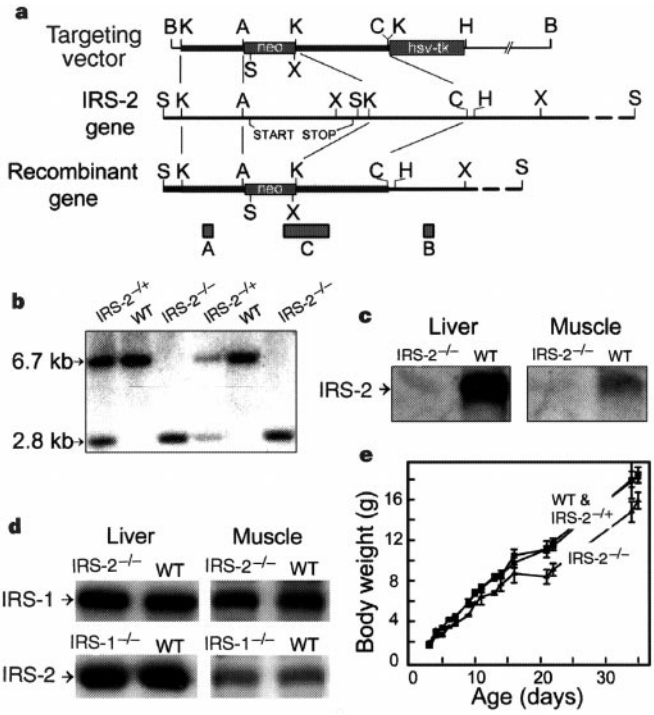

Figure 1 Gene targeting of the IRS-2 locus. **a**, Restriction map of the targeting vector (top), the IRS-2 gene (middle) and the homologous recombinant gene (bottom). Targeted deletion of the entire IRS-2 gene and its replacement with the PGK/neo cassette was done using the targeting vector. Restriction enzymes are as follows: A, *Apa*1; B, *Bcl*1; C, *Cla*1; H, *Hin*dIII; K, *Kpn*1; S, *Spe*1; X, *Xma*1. Probes A–C were used to screen for homologous recombination by Southern blotting. **b**, Southern-blot analysis from homozygous mutant mice (*IRS-2*$^{-/-}$), heterozygotes (*IRS-2*$^{-/+}$) and wild-type animals (WT). Tail DNA was digested with *Spe*1 and analysed by Southern blotting with a 0.3-kilobase (kb) external genomic fragment (probe A). A 6.7-kb fragment is indicative of the wild-type allele and a 2.8-kb fragment is indicative of the recombinant allele. **c**, Immunoprecipitatin and western-blot analysis of liver and muscle, showing lack of IRS-2 protein in *IRS-2*$^{-/-}$ mice. Each lane represents tissue from one animal and represents three independent experiments. **d**, Immunoprecipitation and western-blot analysis of the liver and muscle expression of IRS-1 in wild-type and *IRS-2*$^{-/-}$ mice, and of IRS-2 in wild-type and *IRS-1*$^{-/-}$ mice. Each lane represents tissue from one animal and represents three independent experiments. **e**, Mean weight ± s.e.m. of WT, *IRS-2*$^{+/-}$ and *IRS-2*$^{-/-}$ animals on a C57B16 × 129/Sv background at the indicated ages (days). Data are from six litters, with a total of at least 15 animals per genotype.

without ketosis, and died from dehydration and hyperosomolar coma; female mice followed a similar disease progression but rarely died. Thus, deletion of IRS-2 progressively impaired glucose tolerance with greater than 95% penetrance, whereas heterozygous and wild-type animals were unaffected.

The progressive development of diabetes in IRS-2-deficient mice suggested that deletion of this gene caused a combination of peripheral insulin resistance and inadequate compensatory insulin secretion because of relative β-cell failure. To determine whether *IRS-2*$^{-/-}$ mice were insulin-resistant, we measured fasting serum insulin levels and determined insulin sensitivity *in vivo*. Insulin levels in wild-type and *IRS-2*$^{-/-}$ neonates were not significantly different, suggesting that *IRS-2*$^{-/-}$ mice were slightly insulin-resistant in light of their increased random glucose levels, mentioned above. However, after 6 weeks *IRS-2*$^{-/-}$ mice exhibited threefold higher fasting insulin levels than wild-type animals, and insulin-tolerance tests showed a significantly reduced hypoglycaemic response to exogenous insulin (Fig. 2c, d).

To define the nature of the insulin resistance, we determined basal and insulin-stimulated whole-body glucose disposal in conscious mice using the euglycaemic hyperinsulinaemic clamp and tracer techniques[8]. Six-to-eight-week-old wild-type and *IRS-2*$^{-/-}$ mice in the fasted state showed identical basal rates of glucose disposal and levels of production of hepatic glucose, despite the presence of hyperinsulinaemia in the *IRS-2*$^{-/-}$ animals. However, low-dose insulin infused at a rate of 2.5 mU kg^{-1} min^{-1} did not increase whole-body glucose disposal or suppress hepatic glucose release in *IRS-2*$^{-/-}$ mice, although this dose of insulin markedly enhanced these effects in wild-type and *IRS-2*$^{+/-}$ mice (Fig. 2e, f). A higher insulin dose (20 mU kg^{-1} min^{-1}) increased glucose disposal and suppressed hepatic glucose production in *IRS-2*$^{-/-}$ mice, confirming that there was profound insulin resistance in both skeletal muscle and liver.

IRS proteins are tyrosine-phosphorylated by the insulin receptor

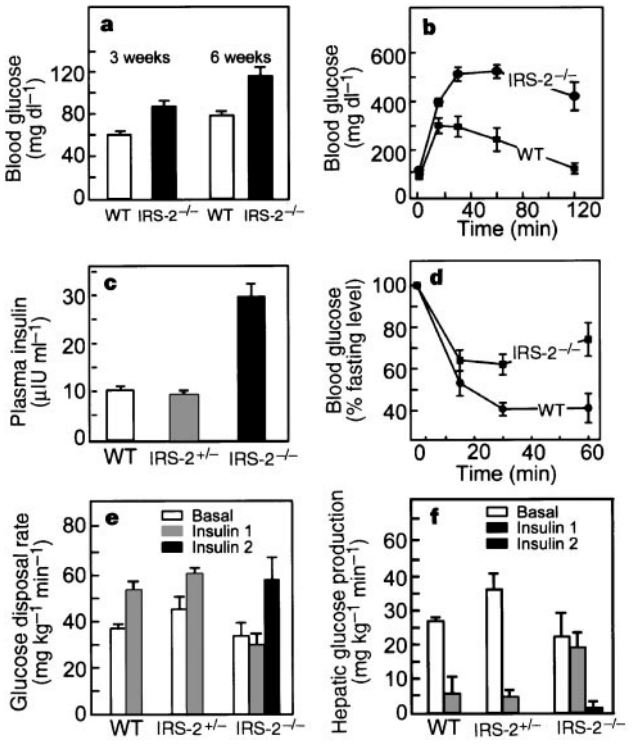

Figure 2 Fasting blood glucose and glucose-tolerance test, fasting insulin levels and insulin-tolerance test, and *in vivo* glucose disposal and hepatic glucose production. **a**, After a 15 h overnight fast, blood glucose levels were determined using a Glucometer Elite glucometer (Bayer). Results are mean values ± s.e.m. for at least eight animals per genotype, with ages as indicated. WT, wild type. **b**, Glucose-tolerance tests after intraperitoneal loading with 2 g D-glucose per kg were performed on 6-week-old animals of the indicated genotype. Results are mean values ± s.e.m. for at least eight animals per genotype. **c**, Serum insulin levels were measured by radioimmunoassay on 4–6-week-old anaesthetized animals after a 15 h overnight fast. Data are the mean values ± s.e.m. for at least 12 animals per genotype. **d**, Insulin-tolerance tests were performed on fed 4–6-week-old animals. Results are expressed as percentage of initial blood glucose concentration and are the mean values ± s.e.m. for at least eight animals per genotype. **e**, Glucose-disposal rate and **f** hepatic glucose production rate were determined on fasted, conscious 8-week-old mice using the euglycaemic hyperinsulinaemic clamp. Basal rates and those stimulated by infusion of insulin at a rate of 2.5 mU kg^{-1} min^{-1} (insulin 1) and 20 mU kg^{-1} min^{-1} (insulin 2) were determined. Results are the mean values ± s.e.m. for three animals per genotype.

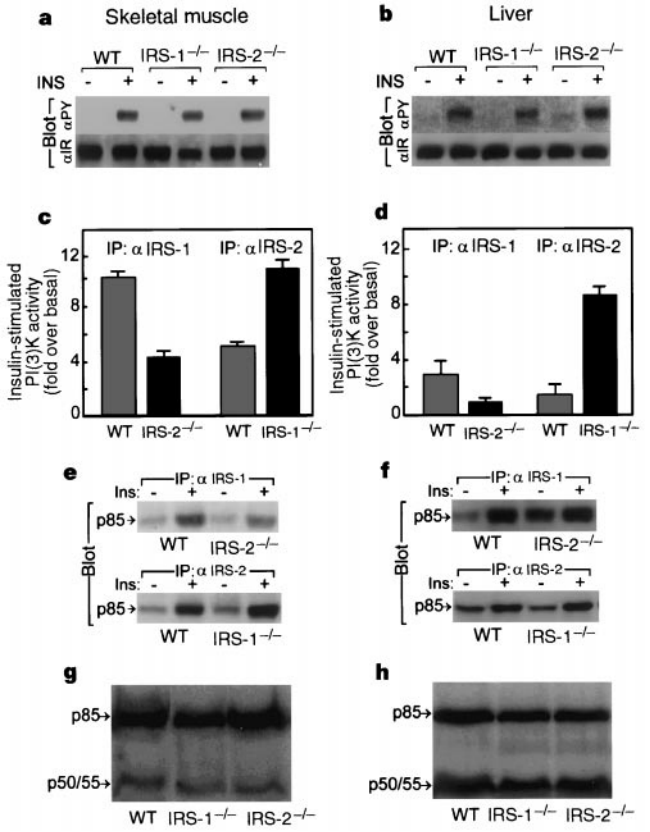

Figure 3 Expression and insulin-stimulated tyrosine phosphorylation of the insulin receptor (IR), insulin-stimulated activation of PI(3)K and IRS association with p85, and expression of PI(3)K adaptor subunits in the liver and muscle of wild-type (WT), *IRS-1*$^{-/-}$ and *IRS-2*$^{-/-}$ mice. Supernatants of muscle (**a**) or liver (**b**) homogenates containing equal amounts of protein from untreated and insulin (INS)-treated 4–6-week-old mice were immunoprecipitated with anti-IRβ antibody and blotted for either antiphosphotyrosine (αPY) or IRβ (αIR). Data are representative of data obtained from three animals per genotype. Supernatants of muscle (**c**) or liver (**d**) homogenates containing equal amounts of protein from untreated and insulin-treated 4–6-week-old mice were immunoprecipitated (IP) in duplicate with the indicated antibody (αIRS-1 or αIRS-2); immunoprecipitates were assayed *in vitro* for PI(3)K activity. Data are the mean values ± s.e.m. of two independent experiments and represent data from a total of eight wild-type, nine *IRS-2*$^{-/-}$ and four *IRS-1*$^{-/-}$ animals. Results are expressed as fold stimulation of activity above that of non-insulin-treated controls (fold stimulation over basal). Muscle (**e**) and liver (**f**) homogenates treated as above were immunoprecipitated with the indicated antibody (αIRS-1 or αIRS-2) and subjected to western analysis to study association with p85α/β. Data are representative of data obtained from three animals per genotype. Ins, insulin. Muscle (**g**) and liver (**h** lysates from animals of the indicated genotypes were subjected to SDS–PAGE and western blotting with an anti-p85 SH2 domain antiserum, which recognize p85α/β and the p50/55 splice variants. Data are representative of those obtained from three animals per genotype.

during insulin stimulation and bind to the Src homology 2(SH2) domains in various effector proteins, including PI(3)K (ref. 9). We examined the proximal steps in this signalling cascade in *IRS-2*$^{-/-}$, *IRS-1*$^{-/-}$ and wild-type mice to determine the potential contribution of any defects in these signalling elements to the development of peripheral insulin resistance. Equivalent insulin-receptor expression and tyrosine phosphorylation of the insulin-receptor β-subunit were seen in both the muscle and liver of *IRS-2*$^{-/-}$ and wild-type mice (Fig. 3a, b). PI(3)K may be involved in mediating several insulin-regulated metabolic pathways, including glucose uptake[10], antilipolysis[11], glycogen synthesis[12] and the suppression of hepatic gluconeogenesis through the regulation of phosphoenolpyruvate carboxykinase (PEPCK) expression[13]. Abnormalities in the activation of PI(3)K could explain defective glucose homeostasis in the *IRS-2*$^{-/-}$ mice. Therefore, the increase in PI(3)K activity after stimulation with insulin of IRS-1 immunoprecipitates from the muscle and liver of *IRS-2*$^{-/-}$ mice was compared with the increase in PI(3)K activity in wild-type animals and contrasted with the PI(3)K activity detected in IRS-2 immunoprecipitates from these tissues from *IRS-1*$^{-/-}$ mice and wild-type mice. The increase in PI(3)K activity associated with IRS-1 upon stimulation with insulin was reduced by >50% in both muscle and liver of *IRS-2*$^{-/-}$ mice as compared with wild-type animals (Fig. 3c, d). The reduction in fold stimulation was due in part to an increase in basal PI(3)K activity in IRS-1 immunoprecipitates from liver and muscle of *IRS-2*$^{-/-}$ mice. These findings suggest a potential defect in the ability of cells to appropriately regulate both basal and insulin-stimulated PI(3)K activity in the absence of IRS-2.

In contrast, the insulin-stimulated PI(3)K activity in IRS-2 immunoprecipitates from the liver and muscle of *IRS-1*$^{-/-}$ animals was markedly enhanced when compared with the IRS-2-associated PI(3)K activity in the tissues of wild-type animals, as previously reported[7]. This pattern of PI(3)K activation in muscle and liver paralleled the insulin-stimulated association of the p85 subunit of PI(3)K with IRS-1 in wild-type and *IRS-2*$^{-/-}$ animals and its association with IRS-2 in wild-type and *IRS-1*$^{-/-}$ mice (Fig. 3e, f). However, no differences in expression of p85α/β, p55^{PIK} and the splice variants p50/55 were detected in the liver and muscle of animals of the three genotypes (Fig. 3g, h). Therefore, the functional defects observed in insulin-stimulated PI(3)K activation in *IRS-2*$^{-/-}$ mice may underlie the abnormalities in glucose metabolism in these animals.

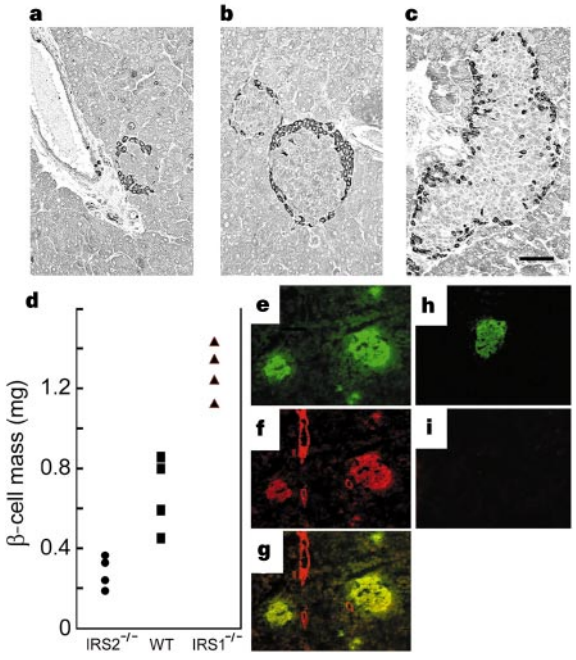

Figure 4 Islet morphology and analysis of β-cell mass in *IRS-2*$^{-/-}$, *IRS-1*$^{-/-}$ and wild-type mice, and expression of IRS-2 in islets of wild-type and *IRS-2*$^{-/-}$ mice. **a**–**c**, Immunostaining for non-β-cell hormones of pancrease sections from 4-week-old male animals. Representative islets from (**a**) IRS-2$^{-/-}$, (**b**) wild-type and (**c**) IRS-1$^{-/-}$ animals are shown and demonstrate the relative differences in islet-cell mass between the animals of each genotype (bar represents 100 μm). **d**, Quantification of β-cell mass by point-counting morphometric analysis on sections from the same mice analysed blind for the genotype. Mean total pancreatic weights (g) ± s.e.m. for each genotype were: wild-type, 178 ± 19; *IRS-2*$^{-/-}$, 123 ± 12; *IRS-1*$^{-/-}$, 113 ± 9 ($n = 4$). **e**–**g**, Immunostaining in wild-type animals for (**e**) insulin, (**f**) IRS-2, and colocalization of both proteins (**g**). **h**, **i**, Immunostaining in *IRS-2*$^{-/-}$ animals for insulin (**h**) and IRS-2 (**i**). Representative fields showing both islets and pancreatic ducts are shown.

Although insulin resistance is important in the early stages of type 2 diabetes in humans, the failure in adequate β-cell compensation leads to the progression to the diabetic state[5]. Compensation for insulin resistance can be achieved either by greater insulin secretion per β-cell or by an increase in β-cell mass through neogenesis or replication of the existing β-cells[14]. Morphometric analysis of pancreases from mice at 4 weeks of age, a time when there is normally a significant increase in β-cell mass[15], showed that *IRS-2*$^{-/-}$ mice had significantly reduced β-cell mass (0.278 ± 0.04 mg) compared with wild-type mice (0.677 ± 0.09 mg), but no significant difference in non-β endocrine-cell mass (Fig. 4a, b, d and data not shown). In contrast, the β-cell mass of *IRS-1*$^{-/-}$ mice, which have insulin resistance without diabetes, was almost double that of wild-type mice (1.280 ± 0.07 mg) (Fig. 4c, d). Subsequent examination of neonatal *IRS-2*$^{-/-}$ pancreas showed relative β-cell deficiency, suggesting that these changes are independent of long-term metabolic effects (data not shown). Functional assessment of insulin release *in vivo* during a glucose-tolerance test showed that 4-week-old wild-type mice (with a fasting glucose level of 79 ± mg dl^{-1}) exhibited a twofold increase in circulating insulin levels (from 11.75 ± 1.4 international microunits (μIU) ml^{-1} to 24.4 ± 2.7 μIU ml^{-1}; $n = 4$) 60 minutes after glucose loading. Similarly, *IRS-2*$^{-/-}$ mice (with fasting glucose levels of 106 ± 5 mg dl^{-1}), despite fasting hyperinsulinemia, responded with a 1.9-fold increase in insulin levels 60 minutes after glucose loading (fasting, 23.5 ± 4.7 μIU ml^{-1}; 60 min, 42.1 ± 5.8 μIU ml^{-1}; $n = 4$). These results indicate that, in the early stages of the development of the diabetic phenotype, glucose-stimulated insulin release may be nearly normal. However, as the hyperglycaemia progresses we see attenuation of glucose-stimulated insulin release, which may be attributed to glucose toxicity towards β-cell function (data not shown).

To obtain further insights into the role of IRS-2 in β-cell function, we studied the expression of this protein in the islets of wild-type animals. Immunofluorescence staining showed that IRS-2 expression co-localized with insulin in the islets, indicating that it may be present in β-cells not non-β cells (Fig. 4a–g). There was also significant IRS-2 staining in the ductal epithelium, which is the site of neogenesis of new islets from ductal precursor cells[14]. IRS-2 staining was absent from the islets and ducts of *IRS-2*$^{-/-}$ mice (Fig. 4h, i). Thus, IRS-2-dependent signalling pathways may be important for the cells that are involved in the proliferative and neogenic responses of the islets.

Our results indicate that deletion of IRS-2 causes the progressive development of a type 2 diabetic phenotype in mice. *IRS-2*$^{-/-}$ mice exhibit mild peripheral insulin resistance and β-cell deficiency at birth but have adequate compensatory insulin secretion for several weeks. However, subsequent relative β-cell failure in the face of continued peripheral resistance causes overt fasting hyperglycaemia without ketoacidosis, the common characteristic of human type 2 diabetes (ref. 5). The mechanisms of peripheral insulin resistance are unknown at present, and the exact contribution of the observed insulin resistance of muscle and liver to the progression of the disease requires further study.

Our results provide insight into the potential differences in the physiological roles of IRS-1 and IRS-2. *IRS-2*$^{-/-}$ mice show marked abnormalities in glucose homeostasis but minimal growth defects, whereas the opposite is the case for *IRS-1*$^{-/-}$ mice. Thus, IRS-1 and IRS-2 cannot be functionally interchanged to produce either IGF-1-stimulated mitogenesis, as has been suggested by previous *in vitro* data[16], or, as we demonstrate, to produce insulin-regulated metabolism. The signalling specificity through IRS-1 and IRS-2 may be accomplished by specific expression patterns and distinct phosphorylation patterns during interaction with various activated receptors[17]. Our observations of PI(3)K activity in muscle and liver show functional differences in the ability of IRS proteins to regulate PI(3)K and implicate IRS-2 as the more critical *in vivo* regulator of this signalling pathway, which mediates many of the metabolic effects of insulin.

The combination of reduced β-cell mass and a failure of islet hyperplasia in the face of insulin resistance and hyperglycaemia distinguishes the *IRS-2*$^{-/-}$ mouse from other monogenic and polygenic models of type 2 diabetes. For example, *IRS-1*$^{-/-}$ mice, or mice with compound heterozygous disruptions of IRS-1 and the insulin receptor[18], develop marked β-cell hyperplasia in response to insulin resistance; this is not seen in human lean type 2 diabetics[19]. Likewise, *IRS-2*$^{-/-}$ mice cannot compensate for insulin resistance in this manner. Our results indicate a unique role for IRS-2 in the regulation of β-cell neogenesis, proliferation and survival. The progressive nature of the diabetes in these mice is due to both insulin resistance and reduced β-cell mass, which prevents adequate compensation. As this combination of features is the hallmark of human type 2 diabetes, functional abnormalities in IRS-2 could be involved in the pathogenesis of this human disease. □

Methods

Preparation of the construct for homologous recombination and generation of IRS-2-deficient mice. We cloned the IRS-2 gene from a 129 mouse genomic library[17]. To construct the targeting vector, two fragments of the genomic DNA flanking the coding region were subcloned at convenient restriction sites into the pPNT vector. We transfected linearized pPNT/IRS-2 into the R1 line of embryonic stem (ES) cells derived from 129 mouse blastocysts. Selection was performed with G418 and ganciclovir, and resistant clones were screened for homologous recombination by Southern blotting using 5′ and 3′ external probes (probes A and B) and by an internal probe (C) derived from the neomycin-resistance gene (*neo*) cassette (Fig. 1a). One cell clone fulfilled the requirements for homologous recombination. Blastocysts from C57B1/6 mice were injected with 10–16 targeted ES cells and implanted into pseudopregnant CD-1 foster mothers as described[20]. Several chimaeric male pups were obtained and mated with C57B1/6 females. Germline transmission was confirmed by Southern blotting and heterozygote offspring were intercrossed to obtain animals homozygous for the deletion of IRS-2. These animals were used in subsequent studies with the animals maintained with a C57B1/129sv hybrid background. The IRS-1 targeting vector was constructed in a similar manner and *IRS-1*$^{-/-}$ animals were maintained on the same genetic background as the IRS-2 animals to facilitate comparison of the *IRS-1*$^{-/-}$ and *IRS-2*$^{-/-}$ phenotypes.

Metabolic studies. Animals were maintained on a normal light/dark cycle and handled in accordance with Joslin Diabetes Center Animal Care and Use Committee protocols. Glucose levels were determined from blood taken from mouse tails using a Glucometer Elite glucometer (Bayer). Blood for plasma insulin levels was taken either by retroorbital bleeds from anaesthetized mice or by tail bleeds. Immunoreactive insulin levels were measured by radio immunoassay using rat insulin (Linco) as a standard. Glucose-tolerance tests were performed on animals after a 15-h overnight fast. Animals were injected with 2 g kg^{-1} of D-glucose intraperitoneally and blood glucose values were determined at the times indicated. Insulin tolerance was tested with fed animals between 14:00 and 16:00. Animals were injected with 0.75 units per kg body weight with human crystalline insulin (Lilly) intraperitoneally. Blood was taken immediately before injection and at the times indicated. Results were expressed as percentages of initial blood glucose concentration.

Euglycaemic hyperinsulinaemic clamps were performed on fasted conscious mice using a two-step clamp technique[8]. [3-^{3}H]glucose was infused throughout the clamp study to determine glucose-turnover rate. After a priming dose, [3-^{3}H]glucose was continuously infused at a rate of <0.08 μCi min^{-1} for 5 h. For basal glucose turnover rate measurements, blood samples were collected at 70 and 80 min after the initiation of [3-^{3}H]glucose infusion. Insulin (Eli Lilly) was infused at a rate of 2.5 mU kg^{-1} for 90 min while 20% dextrose was infused by variable infusion pump. Blood samples were collected from tail-tip bleeds for glucose estimation every 10 min. Plasma glucose was clamped at 100 mg dl^{-1}. While glucose levels remained steady, two blood samples were taken for [3-^{3}H]glucose-specific-activity determination. The insulin infusion rate was then increased to 20 mU kg^{-1} min^{-1} for 90 min. Analysis of [3-^{3}H]glucose measurements and calculation of glucose-disposal rates and hepatic glucose production rates were performed as described[8].

Immunoprecipitations, western blotting and PI(3)K assays. Liver and muscle tissue lysates were removed and homogenized at 4 °C as described[7]. The homogenates were solubilized for 1 h at 4 °C and clarified by centrifugation at 15,000 r.p.m. for 30 min. Supernatants containing equal amounts of protein were immunoprecipitated for 2 h with an anti-IRS-2 antibody raised against a glutathione-*S*-transferase (GST)-fusion protein containing residues 619–746 of murine IRS-2, anti-IRS-1 antibody raised against a GST-fusion protein containing residues 735–900 of murine IRS-1, or an antibody against insulin receptor subunit β. Immune complexes were collected with 100 μl of a 50% slurry of protein-A–sepharose resolved on 7.5% SDS–PAGE and transferred to nitrocellulose. The blots were probed with polyclonal antibodies against IRS-1 and IRS-2 and anti-p85 SH2 domain, which recognizes p85α/β, p55^{PIK} and the p50/55 splice variants[21]. Subsequent detection was by either [^{125}I]protein A or enhanced chemiluminescence. For assays of p85 association with IRS proteins and PI(3)K enzymatic activity, 5 units of human insulin were injected as a bolus into the inferior vena cava of anaesthetized mice and the liver, gastrocnemius and quadriceps muscles were removed at 1, 2.5 and 3 min after insulin injection. They were homogenized and solubilized, and supernatants containing equal amounts of protein were immunoprecipitated for 2 h with anti-IRS-2 or with anti-IRS-1C antibodies. Immune complexes were collected and washed extensively and the PI(3)K reaction was performed as described[7]. [^{32}P]incorporation was quantified using a Phosphorimager (Molecular Dynamics).

Immunochemistry and immunofluorescence. Animals were killed by administering an overdose of sodium amytal. The pancreases were removed, cleared of fat and lymph nodes, weighed, and, for immunochemistry, were fixed in Bouin's solution and embedded in paraffin. Sections (of 5 μm) were immunostained for the endocrine non-β-cells, using a cocktail of antibodies (rabbit antibodies against bovine glucagon, against synthetic somatostatin and rabbit against bovine pancreatic polypeptide[15]). β-cell mass was determined by point-counting morphometry as described[22] at a final magnification of ×420, with at least 175 fields being quantified per animal. For immunofluorescence, pancreases were snap-frozen, and 5-μm cryosections were cut and fixed in paraformaldehyde. Sections were permeabilized with 0.2% Triton X-100 and stained with anti-IRS-2 antisera and guinea pig antibodies against porcine insulin, and detection was performed with rhodamine- and fluorescein-conjugated secondary antibodies.

Received 24 November; accepted 29 December 1997.

1. Myers, M. G. Jr & White, M. F. Insulin signal transduction and the IRS proteins. *Annu. Rev. Pharmacol. Toxicol.* **36,** 615–658 (1996).
2. Araki, E., Lipes, M. A., Patti, M. E., Bruning, J. C., Haag, B. L. III, Johnson, R. S. & Kahn, C. R. Alternative pathway of insulin signalling in mice with targeted disruption of the IRS-1 gene. *Nature* **372,** 186–190 (1994).
3. Tamemoto, H. *et al.* Insulin resistance and growth retardation in mice lacking insulin receptor substrate-1. *Nature* **372,** 182–186 (1994).
4. Warram, J. H., Rich, S. S. & Krolewski, A. S. *Joslin's Diabetes Mellitus* (eds Kahn, C. R. & Weir, G. C.) 201–215 (Philadelphia, Lea & Febiger, 1994).
5. DeFronzo, R. A., Bonadonna, R. C. & Ferrannini, E. Pathogenesis of NIDDM: a balanced overview. *Diabetes Care* **15,** 318–368 (1992).
6. Sun, X. J. *et al.* Role of IRS-2 in insulin an cytokine signalling. *Nature* **377,** 173–177 (1995).
7. Patti, M. E. *et al.* 4PS/IRS-2 is the alternative substrate of the insulin receptor in IRS-1 deficient mice. *J. Biol. Chem.* **270,** 24670–246673 (1995).
8. Ren, J. M. *et al.* Overexpression of Glut4 protein in muscle increases basal and insulin-stimulated whole body glucose disposal in conscious mice. *J. Clin. Invest.* **95,** 429–432 (1995).
9. Backer, J. M. *et al.* Association of IRS-1 with the insulin receptor and the phosphatidylinositol 3′-kinase. Formation of binary and ternary signaling complexes in intact cells. *J. Biol. Chem.* **268,** 8204–8212 (1993).
10. Cheatham, B. *et al.* Phosphatidylinositol 3-kinase activation is required for insulin stimulation of pp70 S6 kinase DNA synthesis and glucose transporter translocation. *Mol. Cell Biol.* **14,** 4902–4911 (1994).

11. Okada, T., Kawano, Y., Sakakibara, T., Hazeki, O. & Ui, M. Essential role of phosphatidylinositol 3-kinase in insulin-induced glucose transport and antilipolysis in rat adipocytes: studies with a selective inhibitor wortmannin. *J. Biol. Chem.* **269,** 3568–3573 (1994).
12. Shepherd, P. R., Nave, B. T. & Siddle, K. Insulin stimulation of glycogen synthesis and glycogen synthase activity is blocked by wortmannin and rapamycin in 3T3-L1 adipocytes: evidence for the involvement of phosphoinositide 3-kinase and p70 ribosomal protein-S6 kinase. *Biochem. J.* **305,** 25–28 (1995).
13. Gabbay, R. A. *et al.* Insulin regulation of phosphoenolpyruvate carboxykinase gene expression does not require activation of the Ras/mitogen-activated protein kinase signaling pathway. *J. Biol. Chem.* **271,** 1890–1897 (1996).
14. Bonner-Weir, S., Scaglia, L., Montana, E., Juang, J. H. & Weir, G. C. in *Diabetes 1994* (eds Baba, S. & Kareko, T.) 179–228 (Excerta Medica Int. Congress, 1995).
15. Scaglia, L., Cahill, C. J., Finegood, D. T. & Bonner-Weir, S. Apoptosis participates in the remodeling of the endocrine pancreas in the neonatal rat. *Endocrinology* **138,** 1736–1741 (1997).
16. Bruning, J. C., Winnay, J., Cheatham, B. & Kahn, C. R. Differential signaling by insulin receptor substrate 1 (IRS-1) and IRS-2 in IRS-1 deficient cells. *Mol. Cell Biol.* **17,** 1513–1521 (1997).
17. Sun, X. J. *et al.* The IRS-2 gene on murine chromosome 8 encodes a unique signaling adapter for insulin and cytokine action. *Mol. Endrocrinol.* **11,** 251–262 (1997).
18. Bruning, J. C. *et al.* Development of a novel polygenic model of NIDDM in mice heterozygous for *IR* and *IRS-1* null alleles. *Cell* **88,** 561–572 (1997).
19. Kloppel, G., Lohr, M., Habich, K., Oberholzer, M., Heitz, P. U. Islet pathology and the pathogenesis of type 1 and type 2 diabetes mellitus revisited. *Surv. Synth. Pathol. Res.* **4,** 110–125 (1985).
20. Papaioannou, V., Johnson, R. in *Gene Targeting: A Practical Approach* (ed. Joyner, A.) Ch. 4, pp. 107–146 (Oxford Univ. Press, Oxford, 1993).
21. Pons, S. *et al.* The structure and function of p55PIK reveals a new regulatory subunit for the phosphatidylinositol-3 kinase. *Mol. Cell. Biol.* **15,** 4453–4465 (1994).
22. Montana, E., Bonner Weir, S. & Weir, G. C. Transplanted beta cell response to increased metabolic demand. Changes in beta cell replication and mass. *J. Clin. Invest.* **93,** 1577–1582 (1994).

Acknowledgements. We thank A. Nagy for R1 cells; M. Ginsberg, M. Petruzelli and M. Taneja for technical support; B. Cheatham for the anti-IRβ antibody. Blastocyst injections were performed in the Core Laboratory of the Diabetes and Endocrinology Research Center, Vanderbilt University. This work was supported by grants from the NIH to G.I.S., S.B.W. and M.F.W. D.J.W. is supported by an MRC (UK) Clinician Scientist Fellowship. D.J.B. was supported by a grant from the JDFI. J.S.G. and D.B. were supported by grants from the Spanish Government.

Correspondence and requests for materials should be addressed to M.F.W. (e-mail: Whitemor@joslab.harvard.edu).

Impaired immunoglobulin gene rearrangement in mice lacking the IL-7 receptor

Anne E. Corcoran, Andrew Riddell, Danielle Krooshoop & Ashok R. Venkitaraman

Medical Research Council Laboratory of Molecular Biology, Cambridge CB2 2QH, UK

To generate the full diversity of antibody heavy-chain genes, hundreds of dispersed germline *V* segments must undergo recombination following *D–J* segment joining. Here we report that this process is regulated by the α-chain of the receptor for interleukin-7, a cytokine that stimulates B-cell lymphopoiesis[1]. *D–J* joining occurs normally in immature B lymphocytes from mice lacking the α-chain of the interleukin-7 receptor (IL-7Rα). But recombination of *V* segments is progressively impaired as their distance increases upstream of *D/J*, causing infrequent rearrangement of most *V* segments, which markedly reduces diversity. This is not simply due to defective cell proliferation or impaired recombinase expression. Rather, germline transcripts from distal, unrearranged *V* segments, a marker of chromatin changes that precede recombination, are specifically silenced. So too is expression of Pax-5, which binds to heavy-chain locus control elements and normally stimulates recombination, suggesting a mechanism for these effects. Thus ligands of the interleukin-7 receptor deliver an extrinsic signal that targets *V* segment recombination in the heavy-chain locus by altering the accessibility of DNA substrates to the recombinase. This mechanism augments the recombinational diversity of the primary antibody repertoire.

B lymphopoiesis is impeded at an early stage in the bone marrow of mice lacking IL-7Rα[1]. The number of progenitor (pro)-B cells undergoing immunoglobulin heavy-chain gene (*IgH*) rearrangement is normal (Table 1). But there is a severe (~10-fold) reduction in precursor (pre)-B cells with complete *IgH* rearrangements, and in surface (s) IgM^+ B lymphocytes when compared to age-matched heterozygous controls (Table 1). This developmental block ensues not only from defective proliferation[1,2], but also from an impediment to *IgH* rearrangements whose basis is undetermined[2].

To examine *IgH* rearrangements, we purified fractions of immature B lymphocytes from IL-$7R^{-/-}$ animals and +/− controls. As only a few cells could be isolated by fluorescent cell sorting (Table 1), genomic DNA was analysed[3] by polymerase chain reaction (PCR) to provide a semiquantitative measure of the relative frequency of recombination events. PCR primers are separated in the germ line (Fig. 1a) but are brought into sufficient proximity for PCR amplification only after a recombination event (Fig. 1b).

*D–J*H recombination proceeds normally without IL-7Rα (Fig. 1c). There is no difference between IL-$7R\alpha^{-/-}$ pro-B cells and +/− controls in the frequency of (*D*)*J*H joins involving 13 of 15 known *D*H segments[4].

In contrast, *V*H–(*D*)*J*H joining is impaired. *V*H segments in *IgH* are grouped into homologous families arranged in clusters (Fig. 1a) across approximately a megabase of DNA upstream of *D* segments and the *J* cluster. Most *V*H segments are located at the extreme 5′ end of this region[5,6] and belong to the large *V*HJ558 family (with an estimated 60–1,000 members). In contrast, the small *V*H7183 family containing only ~25 members is adjacent to *D*H segments at its 3′ end. Rearrangements involving these *V*H segment families were distinguished by a PCR assay whose specificity was verified (Fig. 2a) using hybridomas harbouring known rearrangements. *V*H to (*D*)*J*H joins involving *V*HJ558 segments are normally the most frequent rearrangements detected in the $sIgM^+$ B lymphocyte fraction[7,8]. Surprisingly, *V*HJ558 rearrangements were barely detectable in IL-$7R\alpha^{-/-}$, $sIgM^+$ cells compared to +/− controls, despite

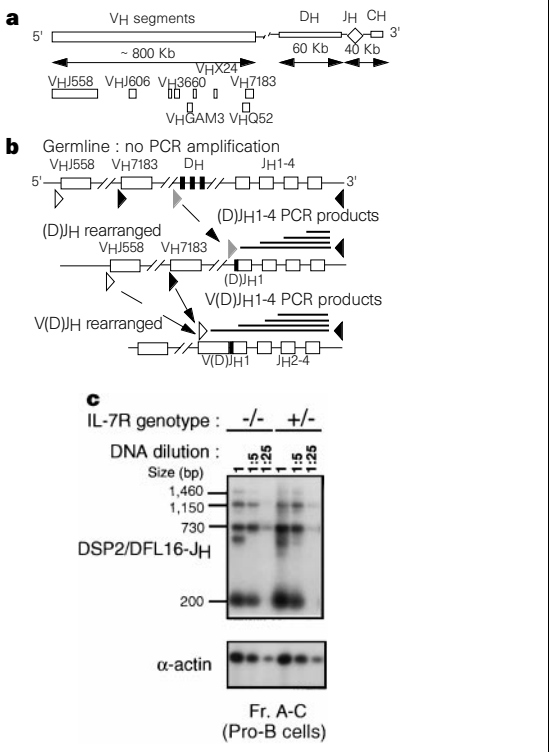

Figure 1 Normal (*D*)*J*H recombination in IL-$7R\alpha^{-/-}$ mice. **a**, The murine *IgH* locus[6], showing approximate map positions of the different *V*H families. **b**, PCR assays used to quantify (*D*)*J*H and *V* to (*D*)*J*H rearrangements. Arrows indicate specific oligonucleotide primers. **c**, There is no difference between IL-$7R^{-/-}$ and IL-$7R^{+/-}$ pro-B cells in the frequency of (*D*)*J*H joining. DSP2/FL16 primers used detect joins involving 13 of 15 known murine *D*H segments. Expected product sizes are indicated.